Available online at www.sciencedirect.com

jmr&t
Journal of Materials Research and Technology
www.jmrt.com.br

Original Article

On the melting of zirconium alloys from scraps using electron beam and induction furnaces – recycling process viability

*Luiz Alberto Tavares Pereira**, *Luis Gallego Martinez*, *Cristiano Stefano Mucsi*, *Luis Augusto Mendes dos Reis*, *Jesualdo Luiz Rossi*

Center for Science and Technology of Materials – CCTM, Nuclear and Energy Research Institute (IPEN - CNEN/SP/USP), Av. Prof. Lineu Prestes, 2242 - CEP 05508-000, São Paulo, SP, Brazil

ARTICLE INFO

Article history:
Received 12 December 2019
Accepted 2 March 2020
Available online 31 March 2020

Keywords:
Zircaloy
Recycling
Electron beam
Induction
Nuclear fuel cladding

ABSTRACT

The pressurized water reactor (PWR) employs UO_2 pellets as nuclear fuel, which are packed in zirconium alloy tubes called nuclear fuel cladding. In the manufacture of the nuclear fuel, machining scraps are generated which are not easily discarded as scraps because of its high cost. These zirconium nuclear alloys are very costly and are not produced in Brazil. In this work, novel methods to recycle Zircaloy scraps using vacuum induction melting and electron beam furnaces were used to obtain ingots. The cast ingots were subjected to thermal treatments and then chemically analyzed, followed by microstructural characterization, mechanical properties evaluation, and X-ray diffraction. The results indicated the feasibility of the processes for obtaining alloys for application in the nuclear area, chemical industry or materials for biological applications such as dental prostheses.

1. Introduction

The nuclear reactor core is comprised of a set of tubes within which are placed the UO_2 pellets and are called fuel element. They are closed at the ends by plug, being produced from massive bars on mechanical lathes, generating large quantities of machining scraps. Both the tube and the cap can be made of Zircaloy-4 (Zry-4). In the Table 1 the typical composition of the Zry-4 alloy used for nuclear fuels is shown [1,2].

The Zircaloy scraps are a valuable source of recycled zirconium, as the Zr metal is the major alloy constituent, with potential value estimated at US $ 78/kg [3–5]. These scraps also have the advantage that Zircaloy is a nuclear grade alloy free from hafnium [1]. Brazil dominates the cycle of nuclear fuel, except for Zircaloy's tubes and bars, which are imported. The price of Zry is determined by global suppliers, and often supply depends on the world scenario of nuclear energy, as each country preserves its own nuclear technology.

The intent of this work is to study the recycling of Zry-4 from machining scraps for nuclear, chemical, or biomedical applications and engineering components [6], since the material cannot be discarded for economic and safety reasons due

* *Corresponding author.*
E-mail: luiz.atp@uol.com.br (L.A. Pereira).
https://doi.org/10.1016/j.jmrt.2020.03.006

Table 1 – Typical nominal chemical composition of Zircaloy-4 alloy [1,2].

Element (% mass)	Sn	Fe	Cr	O	Hf	Zr
Zircaloy-4	1.2–1.7	0.18–0.24	0.07–0.13	0.12	<1000 ppm	balance

to the pyrophoric characteristics of the material. This can reduce costs in the manufacture of fuel rods and the adoption of cleaner technology, being a recycling process with the reuse of material. This work will also study the behavior of these scraps in melting processes, especially vacuum induction melting and provide knowledge for the installation of this type of equipment in the Institute of Energy and Nuclear Research (IPEN). Finally this work aims to propose a means of reducing the volume of Zircaloy scraps currently stored in the Nuclear Industries of Brazil (INB). This volume can potentially be reduced by about 30 times, releasing factory storage area.

The means to achieve these objectives were: a) melting of the scraps using two types of furnaces: electron beam and vacuum induction; b) heat treatment to modify as-cast structure and improve the mechanical properties of the material; c) microstructural characterization, mechanical properties and X-ray diffraction – XRD evaluation.

The electron beam (EB) melting occurs by the generation of an electron beam in an generator, the beam being obtained by the emission of free electrons and their subsequent acceleration under an electrostatic field [7]. When the beam collides with the material to be processed, the kinetic energy of the electrons is deposited into the target, converting beam energy into bulk thermal energy, leading to melting [8]. The vacuum induction melting (VIM) is carried out by electromagnetic induction heating using a variable magnetic field to induce Eddy currents in the material to be heated. These currents are dissipated, leading to heating in the material. This process is only suitable for electrically conductive materials such as metals. This current is supplied by the induction generator which, in turn, generates a surface current in the material by means of electromagnetic induction [9]. Thus, the heating is generated by the vibration and friction of the atoms in the magnetic material through the alternating flow of electric current [10,11].

The heat treatment was carried out to verify the influence of the thermal processing on the mechanical and microstructural properties, since several studies [12–14] have shown changes in mechanical strength due to the behavior of the alpha (α) and beta (β) phases and microstructural features such as second phase precipitates (SPP) or intermetallics.

At 865 °C, Zr undergoes an allotropic transformation from the low temperature hexagonal close packed phase (α phase) to body centered cubic (β phase). On cooling, the transformation is either martensitic or bainitic, depending on the cooling rate, with a strong epitaxy of the α platelets on the old β grains [14,15]. Homogenizing in the beta range causes the alloying elements in second phase particles to dissolve completely in the beta matrix, and the grains grow significantly. Upon quenching, the β grains transform to α needles with separation of the β stabilizing elements to the grain boundaries. As the beta grains cool down, depending on the conditions and the simultaneous growth of the variants orientation relationship lead to the basketweave structure, where the plates cross each other. Another structure's morphology is the parallel-plate, whose structure is composed of a number of long plates and grows from the parent β-grain boundaries. Both of them are called Widmanstätten structure [16], shown in the Fig. 1. It is attributed this difference to the presence of randomly dispersed second phase particles which can to nucleate the α phase plates and to produce a basketweave structure [17].

In the case of Zircaloy, it is possible to find compounds of the Zr-Cr-Fe type with rectangular or spherical morphology in a hexagonal crystal structure (type $ZrCr_2$). This compounds appear in Zry-4 and are small precipitates (less than 0.5 μm in diameter) of the intermetallic $Zr(Fe,Cr)_2$ Laves phase (structure C14) [18,19].

The presence of extrinsic elements in the alloy affect the stability of the α and β phases. Oxygen, nitrogen, carbon and tin are α-phase stabilizers, while iron and chromium are β-phase stabilizers. At room temperature, the alloys consist of a matrix of α-Zr and the solid solution of the alloying elements [15]. The β-quenching results in a solid solution of supersaturated α-Zr in the martensitic form. If the cooling rate is high

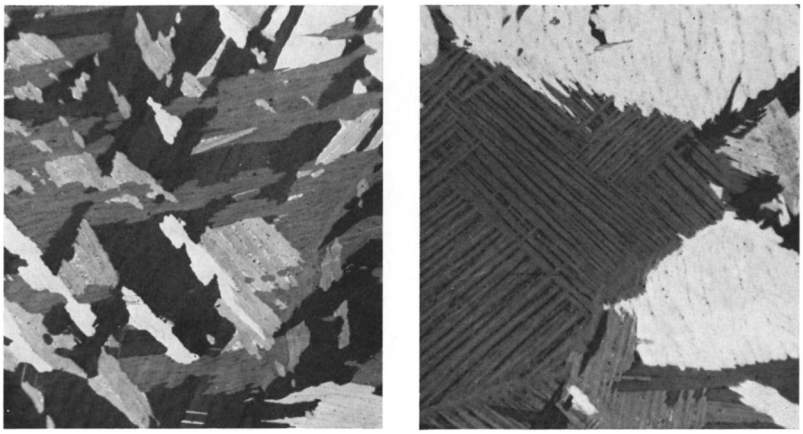

Fig. 1 – Microstructures of Zircaloy-4 showing the Widmanstätten morphologies: (a) basketweave structure; (b) parallel plate structure [17].

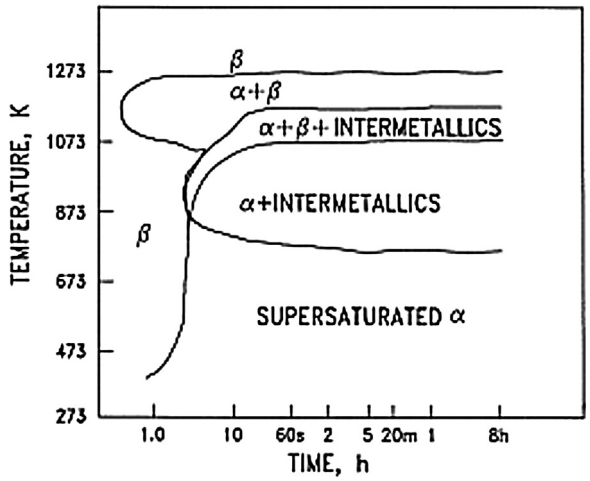

Fig. 2 – Isothermal time-transformation diagram for Zircaloy-2 [13].

enough, it is possible to obtain this structure without secondary phases. Otherwise, precipitation of intermetallics may occur (30 s at 820 °C), as shown in Fig. 2.

A Zry-2 time-temperature transformation diagram (TTT diagram) is shown because the Zry-4 diagram was not available in the researched literature. Since the heat treatment is carried out at a relatively high temperature, the material is subject to oxidation [20]. Traces of oxygen and nitrogen present in the metal greatly affect the rate of oxidation. In the study done by Baek [21] on the oxidation kinetics of Zry-4 between 700 °C and 1200 °C through thermal gravimetric analysis TGA, it was found the growth of alloy grains and the formation of micro cracks, which can affect the mechanical properties of the material [22] and then the alloy must be protected with controlled atmosphere in order not to harm the mechanical properties, as it will be seen in item 2.1.

2. Materials and methods

Before melting, the Zry-4 scraps were prepared as follows and the next subject describes the methods used in this work.

2.1. *Melting*

2.1.1. *Conditioning of Zry-4 scraps*

The treatment consisted of an initial stage of cleaning (washing, degreasing and pickling), followed by the compaction of the machining scraps into briquettes [23] for the melting purposes.

2.1.2. *Melting*

For the EB melting, the used equipment was regulated to 11 kV and 0.3 A to the electron beam established under 6×10^{-5} Torr vacuum, having been charged with 220 g of compacted Zry-4 scraps. An as-cast button was melted with 66 mm diameter and 14 mm thickness. A graphite crucible was used in the melting of the Zircaloy scraps by VIM, where 450 g of briquettes were loaded. The temperature reached was 1824 °C, which melted the load and gave rise to a button 60 mm in diameter and 20 mm in height. The vacuum applied was 7×10^{-1} Torr. Melting in this method lasted about 50 min, while in the former it was faster (approximately 5 min).

2.1.3. *Specimens preparation*

The tensile test specimens were prepared in the sub-size scale (ASTM standard [24]). From the billet melted using electron beam, it was obtained cylindrical bars (4 mm diameter) by wire electro erosion and then 2.5 mm cylindrical specimens were lathe machined. In the induction cast button, blades were cut (1 mm thickness) by diamond discs in a precision cutter, being machined prismatic specimens 4 mm large. These specimens are shown in the Fig. 3. As it was mentioned previously, in order to avoid oxidation during the heat treatment, the specimens were encapsulated in quartz tubes with a vacuum of 220 Torr.

2.1.4. *Heat treatment*

The heat treatment consisted of two stages. First, 4 test encapsulated specimens were subjected to heating (10 °C per minute ramp) to 950 °C, maintained for 2 h. Three specimens were rapidly cooled in water (quenching), i.e., they were withdrawn from the furnace and the encapsulation being broken immediately inside the water. The fourth specimen was kept in the furnace for slow cooling (annealing). In the second step, 2 quenched specimens were re-encapsulated. They were then placed in the furnace initially set at 500 °C for 1 h, and then it

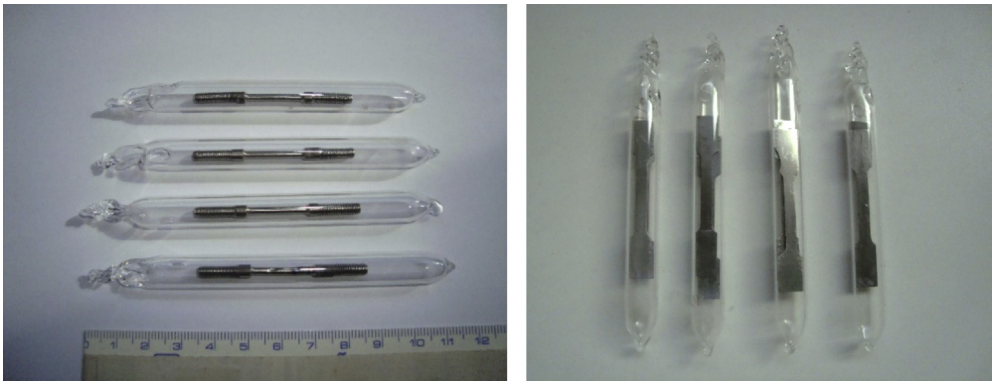

Fig. 3 – Cylindrical and prismatic specimens encapsulated in quartz glass for heat treatment.

Table 2 – Results of chemical and gaseous analysis of electron beam (EB) and vacuum induction (VIM) samples.

Element (% mass)	Scraps	Sample EB	Sample VIM	Specif. Zry-4 [2]
Zr	Balance	Balance	Balance	Balance
Sn	1.246 ± 0.10	1.00 ± 0.03	0.93 ± 0.04	1.20–1.70
Fe	0.213 ± 0.03	0.14 ± 0.01	0.20 ± 0.01	0.18–0.24
Cr	0.080 ± 0.01	0.08 ± 0.04	0.16 ± 0.02	0.07–0.13
Hf	(0.480 ± 0.06) x10^{-2}	0.01 ± 0.00	0.13 ± 0.04	<0.1
H (ppm)	57	11	16	<25
N (ppm)	1299	50	750	<80
O (ppm)	Nd	1640	2030	-*
C (%)	0.16	0.02	0.16	<0.27

Nd, not determined; *, not available.

Table 3 – Mechanical properties of the zirconium alloys obtained by the EB and VIM methods.

Heat treatment	UTS obtained (MPa)	Elongation obtained (%)	UTS ASTM (MPa) [2]	Elongation ASTM (%) [2]
Melting by electron beam				
Annealing	562	12.9	385	18
Quenching	nd	13.3	–	–
Aging 500 °C	662	14.2	–	–
Aging 700 °C	357	nd	–	–
Melting by vacuum induction				
Annealing	566	13.8	385	18
Quenching	701	11.2	–	–
Aging 500 °C	414	16.0	–	–
Aging 700 °C	666	14.4	–	–

nd, not determined; -, not specified.

was removed and subjected to air cooling (aging). The furnace controller was then set to 700 °C, also with a 1-h threshold, when the second specimen was removed for cooling in the air.

2.2. *Chemical, mechanical and microstructural characterization*

2.2.1. *Chemical analysis*

The chemical composition of the samples was determined by the energy dispersive X-ray fluorescence spectrometry (EDXRFS) technique [25]). The chemical analysis was performed using the inert gas technique as an elemental analyzer.

2.2.2. *Tensile testing*

For the cylindrical specimens, two adapters were threaded in the upper and lower grips, whose load (kgf) and displacement (mm) data were recorded on the machine computer. In the case of prismatic specimens, a machine containing appropriate grips was used, whose program converted the data into tension (MPa) and elongation (%), applying a 0.5 mm/min rate in the crossbar displacement.

2.2.3. *Hardness testing*

Hardness measurements were performed on a 100 kgf load durometer on the Rockwell B scale (HR_B). Measurements were made in three regions, respecting the minimum distance between them according to the ASTM standard [26].

2.2.4. *Preparation and microstructural analysis*

The samples were taken using a diamond disc and embedded in polyester resin, being ground with SiC sanding paper with grit size of P400 to P4000 and diamond polishing of 6 μm and 1 μm, finished with colloidal silica 0.06 μm. The etch was performed with a solution of 50% H_2O_2 + 25% HNO_3 + 25% ethyl alcohol + 2 HF drops [27].

2.2.5. *X-ray diffraction*

The X-ray diffraction measurements were performed on a diffractometer using Cuk$_\alpha$ radiation at 40 kV and 30 mA. The results interpretation was carried out using the Crystallographica Search-Match [28] and the Powder Diffraction File of the International Center for Diffraction Data (PDF2/ICDD) [29].

3. Results

The results obtained in this work are presented in the following items.

3.1. *Chemical analysis*

The contents of the main elements of zirconium alloys are listed in Table 2. The specification ASTM B351-08 [2] was included.

3.2. *Tensile testing*

The values of the mechanical properties of zirconium alloy obtained in the two methods are shown in Table 3. In Fig. 4 (a, b)

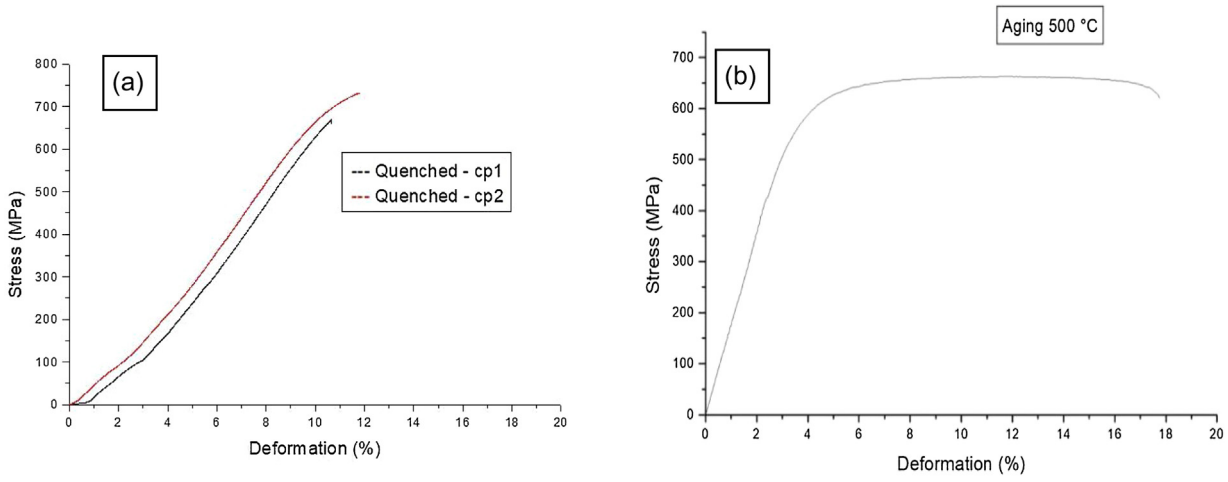

Fig. 4 – Stress versus deformation curves. a) Quenched specimens from vacuum induction melting – VIM; b) aged at 500 °C specimens from electron beam melting – EB.

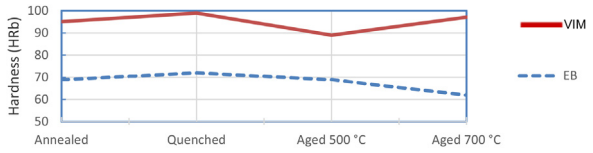

Fig. 5 – HR_B hardness variation according to the heat treatment, annealing, quenching, aging for the samples after vacuum induction melting – VIM; and electron beam melting – EB.

the typical stress versus elongation curves of the heat-treated specimens are shown.

3.3. *Hardness testing*

In Fig. 5, it is possible to observe the influence of the heat treatments on the hardness of the alloys.

3.4. *Microstructural analysis*

3.4.1. *Optical microscopy*

The images of Figs. 6–9 are related to the microstructures of the samples taken from the specimens that received the heat treatments mentioned in item 2.2, comparing the melting methods performed (a, b).

3.4.2. *After annealing*

The characteristic morphology of the Widmanstätten structure [30], specifically basketweave form can be seen in this microstructure (Fig. 6) in both samples and the second phase particles presence in (b), as found in references [18,13].

3.4.3. *After quenching*

After quenching in the alloy obtained by electron beam, the Widmanstätten/basketweave morphology and the presence of large needles of martensite are noted. In the material produced by induction is a thin matrix of Widmanstätten/basketweave structure and α phase needles distributed in the matrix (Fig. 7).

3.4.4. *After aging at 500 °C*

The materials melted by the two methods resulted in similar microstructures, i.e., Widmanstätten fine morphology with α-phase martensite needles and rectangular and round precipitates [31]. There is a small difference between the microstructures related to the type of parallel plates in the first case (Fig. 8a) and basketweave in the second, besides the well-characterized grain boundary (Fig. 8b).

3.4.5. *After aging at 700 °C*

In the billet obtained by electron beam, the presence of the very thin Widmanstätten matrix and well-developed α-phase rectangular and round precipitates are noted. In relation to the alloy obtained by induction, the matrix is similar to the previous one, differentiating itself in the α-phase needles morphology, as shown in Fig. 9.

3.4.6. *Scanning electron microscopy (SEM)*

In Fig. 10, the typical microstructure of the material in the as-cast state of melting observed in the SEM and the semi-quantitative energy dispersive chemical analysis (EDS) of the light region, respectively, are shown.

3.4.7. *X-ray diffraction*

In Fig. 11 can be seen the X-rays diffractogram obtained from the analysis of samples of the cast button via electron beam.

4. Discussion

As for the chemical composition, the contents of chromium and hafnium are higher in the molten alloy by induction compared to the electron beam melting, considering that it is due to the variation of the chemical composition of the raw material. In relation to the gas analysis, due to the smaller suction power of the vacuum system in the induction process, there was greater oxidation of the molten material because

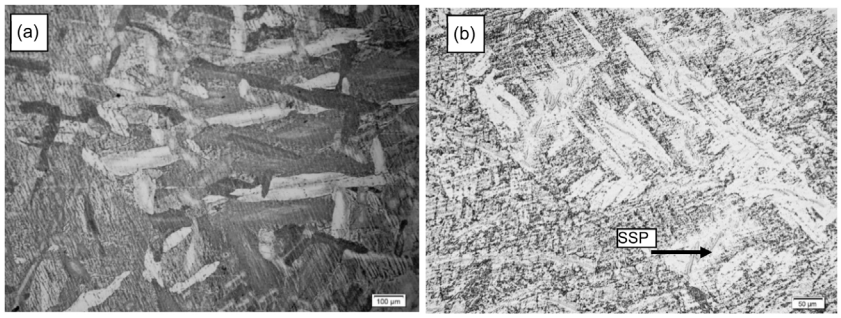

Fig. 6 – Optical micrographs of the microstructures after annealing. (a) Electron beam melting – EB. (b) Vacuum induction melting – VIM, characterized by Widmanstätten structure in basketweave form and the presence of second phase particles.

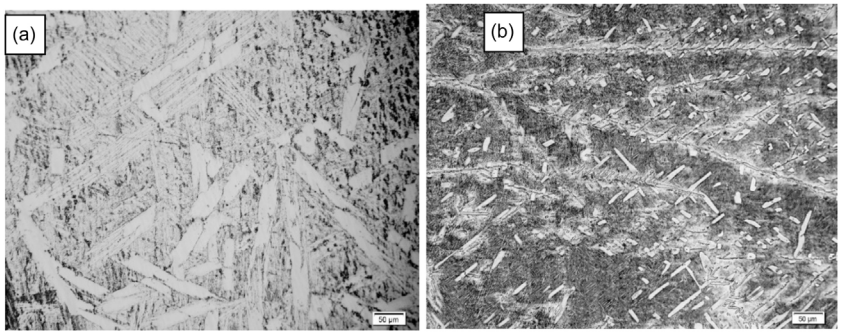

Fig. 7 – Optical micrographs of the microstructures after quenching. (a) Electron beam melting – EB. (b) Vacuum induction melting – VIM. Microstructures with Widmanstätten/basketweave morphology.

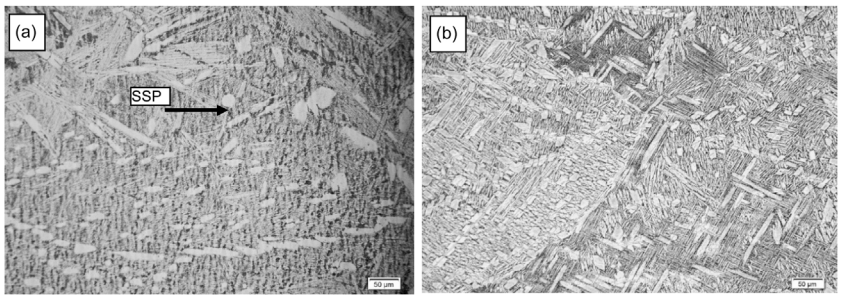

Fig. 8 – Microstructures after aging at 500 °C. (a) EB melting, noticing the presence of particles. (b) VIM melting. Widmanstätten morphologies with martensite needles and rectangular and round precipitates.

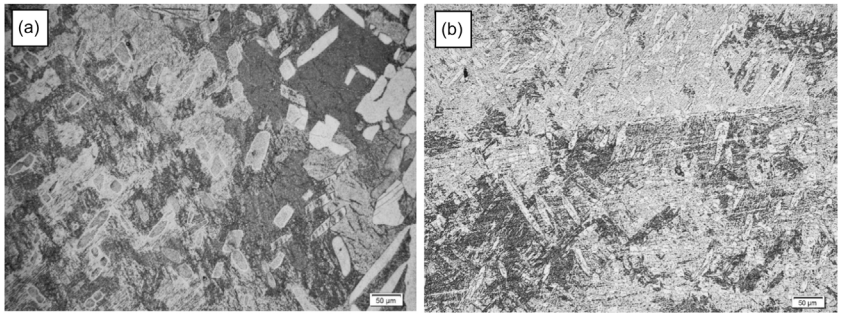

Fig. 9 – Microstructures after aging at 700 °C. (a) EB melting, noting the Widmanstätten matrix and α-phase rectangular and round precipitates. (b) VIM melting, similar morphology, but in the form of needles.

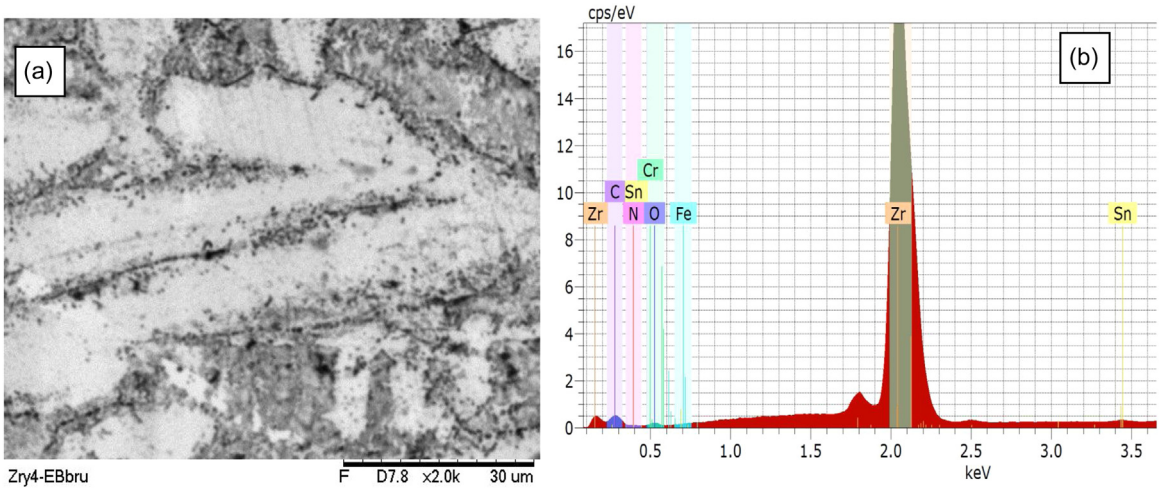

Fig. 10 – (a) SEM micrograph of the alloy obtained by the EB method. (b) Spectrum of the EDS analysis of the light region in (a), indicating the presence of zirconium.

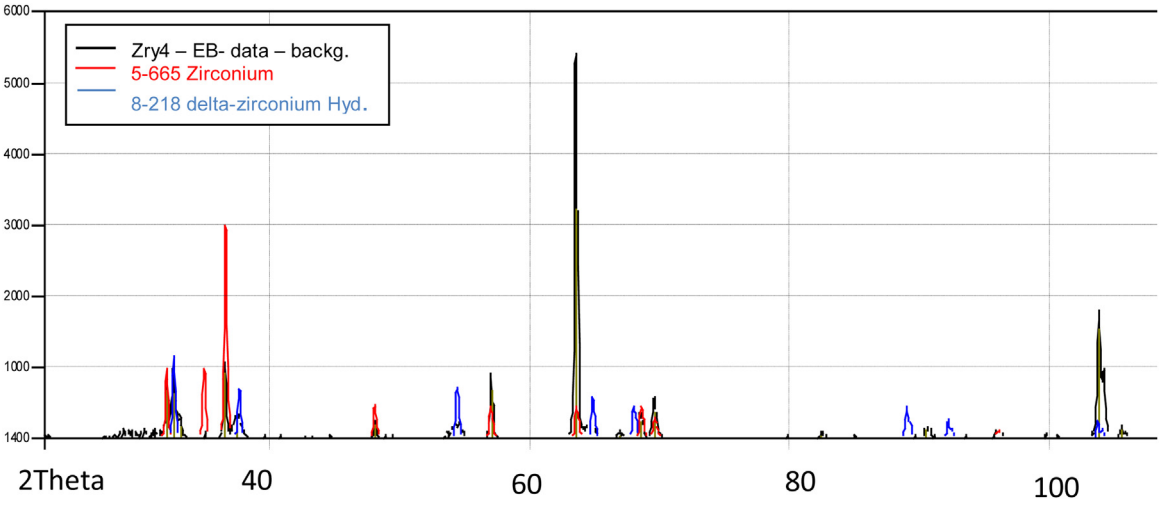

Fig. 11 – X-ray diffraction of the sample melted by electron beam, where the zirconium and zirconium hydride phases are identified.

of the oxygen presence in the atmosphere. During annealing, due to the high temperature and the low cooling rate, the α-phase with Widmanstätten/basketweave structure had the opportunity to precipitate and coarsen. This phase becomes second phase particles, as shown in Fig. 6 (b) [1]. In quenching, according to the TTT diagram (Fig. 2), the formation of the martensitic microstructure is expected and the solutes (Fe, Sn and Cr) are in solid solution [14]. The microstructure of the electron-beam material corresponds to the acicular microstructure and, in the induction melted material, the matrix with thin plates of Widmanstätten/basketweave and the mixture of β-phase needles with rectangular precipitates were found, increasing the magnitude of the mechanical properties. This alloy containing more oxygen, which is an α-phase stabilizer, forms the interstitial solid solution and increases the strength of the material due to the solid solution hardening [16]. Analyzing the TTT diagram shown in Fig. 2, around 500 °C the martensitic microstructure can be obtained and the presence of fine precipitates from supersaturated α-phase can be retained. The hardness increases with increasing temperature of aging due to the presence of intermetallic particles, reaching a maximum around 500 °C and then decreasing in the higher temperatures [15]. At this temperature, 30 s is the time for precipitation to start (in this study, this time was greater than 30 s). In Fig. 9a, can be seen a refined Widmanstätten/basketweave microstructure, containing α-phase precipitates larger and rounded disseminated in the matrix. At higher aging temperatures there is the possibility of martensite dissociation and the formation of isolated α-phase sites. The decrease in the mechanical properties of the alloy obtained by electron beam can be explained due to the maximum at 500 °C mentioned above, from which the precipitates are reduced. In the induction melted alloy, the increase in mechanical properties was possibly influenced by the presence of α-phase needles combined with the higher oxygen content. In relation to the inclination of the curves, it

is a little more pronounced probably due to the accommodation of the prismatic specimens in the fixing machining testing grips.

5. Conclusion

The methods used to melt the Zircaloy machining scraps – electron beam (EB) and vacuum induction (VIM) – were effective to obtain alloys having suitable chemical characteristics, microstructure and mechanical properties. In the first method (EB), the melt as a function of charge quantity was fast, while the second method (VIM) was a comparably slower melting process. Furthermore, the first process has a more efficient vacuum system and lead to lower alloy oxidation. In fact, the induction method was shown to melt the Zry-4 eliminating the doubt that it would not be a proper process to melt this kind of material because it is not magnetic. In reality it only needs adjustments concerned to the process parameters (frequency, time and etc.) and the control of the vacuum system to minimize the oxygen in the atmosphere. The specimens for the tests were scaled for sub-size according to the size of the cast billets. It was important to adopt the standardized dimensions and the format dictated in the ASTM E8 of the specimens in order not to influence the tests, obtaining reliable results. The encapsulation of the specimens was also very important, as it avoided the material oxidation, preserving the surface integrality. Surface defects are initiators and propagators of microcracks, then interfere with mechanical properties and it also affects the hardness measurements. The heat treatments were based on the Zry-2 TTT diagram. Although it is from Zry-2, it was used for Zry-4 successfully and proved to be a very good tool for obtaining the desired microstructure and achieve its properties. Although it is very common TTT for steels, there are few studies involving zirconium alloys TTT diagrams. The mechanical properties (tensile strength and elongation) in the induction melting method resulted in higher values in relation to the electron beam method. Induced and quenched cast material reached the highest strength limit, although the elongation was below that specified in ASTM. The highest elongation value reached (and close to ASTM values) occurred with the material obtained by induction and aged at 500 °C. This work has shown two viable methodologies to recycle Zry-4 scraps into usable ingots. This provides the basis for experimental scale-up to demonstrate the macroscale feasibility of such processes, which could lead to dramatic cost reductions in the utilization of LWR cladding in Brazil.

Conflicts of interest

The authors declare no conflicts of interest.

Acknowledgements

The Technological Research Institute of State of São Paulo (IPT). To the Institute of Aeronautics and Space (IAE/CTA). To the Institute of Physics of the University of São Paulo (USP). To the National Council of Scientific and Technological Development (CNPq) for Pereira L.A.T. scholarship.

REFERENCES

[1] Bohe AE, Andrade Gamboa JJ, Lopasso EM, Pasquevich DM. Zirconium recovery from Zircaloy shavings. J Mater Sci 1996;31:3469–74.
[2] ASTM International. Standard specification for hot-rolled and cold-finished zirconium and zirconium alloy bars, rod, and wire for nuclear application. ASTM: B351-08. ASTM-American Society for Testing and Materials.
[3] Dayton RW, Allen CM, Eberts WU. The reclamation of zirconium machining chips to produce arc-melting feed stock. United States Atomic Energy Commission; 1952 (AECD-3499).
[4] Mimura K, Lee S-W, Isshiki M. Removal of alloying elements from zirconium alloys by hydrogen plasma-arc melting. J Alloys Compd 1995;221(1–2):267–73.
[5] Collins ED, Delcul GD, Spencer BB, Brunson RR, Johnson JA, Terekhov DS, et al. Process development studies for zirconium recovery/recycle from used nuclear fuel cladding. Procedia Chem 2012;7:72–6.
[6] Yan X, Zhang Y. A body-centered cubic Zr50Ti35Nb15 medium-entropy alloy with unique properties. Scr Mater 2020;178:329–33.
[7] Schiller S, Heisig U, Panzer S. Electron beam technology. John Wiley & Sons, Inc.; 1980. p. 30–2.
[8] Choudhury A, Hengsberger E. Electron beam melting and refining of metals and alloys. ISIJ Int 1992;32(5):673–81.
[9] Cheremisinoff NP. Electromagnetic induction heating. In: Electrotechnology – industrial and environmental applications. William Andrew Inc.; 1996. p. 1–21.
[10] DaWei Induction Heating Machine Co., Ltd. Disponível em: <http://www.induction-heating.com.cn/>. Acesso em: 15 jun 2019. Available from: http://www.induction-heating.com.cn/.
[11] Ščepanskis M, Jakovičs A, Baake E, Nacke B. Solid inclusions in an electromagnetically induced recirculated turbulent flow: simulation and experiment. Int J Multiph Flow 2014;64:19–27.
[12] Meng X, Northwood D. Second phase particles in Zircaloy-2. J Nucl Phys Mater Sci Radiat Appl 1989;168:125–36.
[13] Jayakumar T, Palanichamy P, Raj B. Detection of hard intermetallics in B-quenched and thermally aged Zircaloy-2 using ultrasonic measurements. J Nucl Phys Mater Sci Radiat Appl 1998;255:243–9.
[14] Olander D, Motta A. Zirconium alloys. In: Light-water reactor materials. Illinois, USA: American Nuclear Society; 2009. p. 1–39.
[15] Kaufmann AR, Ttt Magel. Physical metallurgy of zirconium and its alloys. In: Lustman B, Kerze FJ, editors. The metallurgy of zirconium. McGraw-Hill Book Co.; 1955. p. 348–423.
[16] Massih A, Andersson T, Witt P, Dahlbäck M, Limbäck M. Effect of quenching rate on the β-to-α phase transformation structure in zirconium alloy. J Nucl Mater 2003; 322(2–3):138–51.
[17] Holt RA. The beta to alpha phase transformation in Zircaloy-4. J Nucl Phys Mater Sci Radiat Appl 1970;35:322–34.
[18] Vizcaino P, Banchik AD, Abriata JP. Synchrotron X-ray diffraction evidences of the amorphization/dissolution of the second phase particles (SPPs) in neutron irradiated Zircaloy-4. Mater Lett 2008;62(3):491–3.
[19] Miquet A, Charquet D, Allibert CH. Solid state phase equilibria of Zircaloy-4 in the temperature range 750-1050 °C. J Nucl Mater 1982;105:132–41.
[20] Kim HH, Kim JH, Moon JY, Lee HS, Kim JJ, Chai YS. High-temperature oxidation behavior of Zircaloy-4 and Zirlo in steam ambient. J Mater Sci Technol 2010;26(9):827–32.

[21] Baek JH, Park KB, Jeong YH. Oxidation kinetics of Zircaloy-4 and Zr–1Nb–1Sn–0.1Fe at temperatures of 700–1200°C. J Nucl Mater 2004;335(3):443–56.
[22] Suárez A, Veiga F, Polvoroza R, Artaza T, Holmberg J, de Lacalle L, et al. Surface integrity and fatigue of non-conventional machined Alloy 718. J Manuf Process 2019;48(November):44–50.
[23] Pereira LAT. Desenvolvimento de processos de reciclagem de cavacos de zircaloy via refusão em forno elétrico a arco e metalurgia do pó. Instituto de Pesquisas Energéticas e Nucleares - IPEN/USP. Doctorate Thesys; 2014 (In Portuguese).
[24] ASTM Int. Standard Test Methods for Tension Testing of Metallic Materials - ASTM E8/E8M. ASTM-American Society for Testing and Materials.
[25] CRM 098. Certified Reference Material BCR-Commission of the European Communities. Brussels, Belgium: Commission of the European Communities.
[26] ASTM E18-15. Standard Test Methods for Rockwell Hardness of Metallic Materials. ASTM–American Society for Testing and Materials.
[27] Vander Voort GF. Metallography – principles and practice. ASM International; 1999.
[28] Crystallographica-Search Match, Oxford Cryosystems Ltd., demo version. Disponível em <http://www.oxcryo.com/cg/csm/>. Acesso em: 09 jan 2014.
[29] Powder Diffraction File – PDF2 versão 2003. International Centre for Diffraction Data.
[30] Danielson PE. Metallographic techniques for zirconium and zirconium alloys. In: Metals handbook. American Society for Metals - ASM; 2004. p. 497–502.
[31] Östberg G. Metallographic study of the isothermal transformation of Beta phase in zircaloy-2, Vol. AE 30. Stockholm, Sweden: Aktiebolaget Atomenergi; 1960.